Characterization of force chains in granular material

J. F. Peters,[1,*] M. Muthuswamy,[2,†] J. Wibowo,[1] and A. Tordesillas[2,‡]
[1]*U.S. Army Corps of Engineers, Engineer Research and Development Center, Vicksburg, Mississippi, 39180 USA*
[2]*Department of Mathematics and Statistics, University of Melbourne, Parkville 3010, Melbourne, Australia*
(Received 5 July 2005; published 21 October 2005)

It has been observed that the majority of particles in a granular material carries less than the average load and that the number of particles carrying larger than the average load decreases exponentially with increasing contact force. The particles carrying above average load appear to form a strong network of forces while the majority of particles belong to a weak network. The strong network of forces appear to have a spatial characteristic whereby the stronger forces are carried though chainlike particle groups referred to as force chains. There is a strong case for a connection between force chains of the discrete medium and the trajectory of the most compressive principal stress in its continuous idealization. While such properties seem obvious from descriptive analysis of physical and numerical experiments in granular media, progress in quantification of the force chain statistics requires an objective description of what constitutes a force chain. A procedure to quantify the occurrence of force chains is built on a proposed definition having two parts: first, the chain is a quasilinear arrangement of three or more particles, and second, along the chain, stress concentration within each grain is characterized by the vector delineating the most compressive principal stress. The procedure is incorporated into an algorithm that can be applied to large particle assemblies to compile force chain statistics. The procedure is demonstrated on a discrete element simulation of a rigid punch into a half space. It was found that only approximately half of the particles within the group of so-called strong network particles are part of force chains. Throughout deformation, the average length of force chains varied slightly but the number of force chains decreased as the punch advanced. The force chain lengths follow an exponential distribution. The procedure provides a tool for objective analysis of force chains, although future work is required to incorporate branching of force chains into the analysis.

DOI: 10.1103/PhysRevE.72.041307 PACS number(s): 83.80.Fg, 45.70.−n, 81.05.Rm, 05.40.−a

I. INTRODUCTION

In a granular material, forces are transmitted from one particle to the next via their contacts. When visualized through stress-induced birefringence within assemblies of photoelastic disks [1–3], the manner of propagation appears as a complex force network that is highly ramified and undergoes rapid changes in branch morphology throughout the material's deformation history. Over the past few decades, there have been numerous attempts made toward the characterization of this force network, with techniques such as contact dynamics simulations [4,5], discrete element simulations [6], the scalar q model of force transmission [7,8] and its variants [9,10], the oriented stress linearity model [11], and models based on statistical mechanics [12], just to name a few. Two key characteristics of the force network have been identified (see, e.g., [13,14]): (1) The majority of particles (typically greater than 60%) carry less than the average force (i.e., "weak network"), and (2) the number of particles carrying larger than the average force (i.e., "strong network") decreases exponentially with increasing contact force magnitude.

Such a heterogeneous structure clearly poses a problem from a continuum mechanics viewpoint since modeling techniques within this framework are based on the assumption that, within a neighborhood of particles, fluctuations of particle properties from their mean are small [15]. For static systems (e.g., a sandpile), there have been some attempts at the development of constitutive models that incorporate or predict force chains (e.g., [16–18]). In particular, the studies of Bouchaud [17] and Socolar [18] on "directed force chain networks" present one of the first attempts at bridging the gap between force chains and the macroscopic response by characterizing the structure of the force network: force chains are considered to be made up of segments which can split up or join, with each segment having a single direction and intensity. Interestingly, if we look at other complex materials, e.g., jammed colloids, a single force chain is modeled as a "linear string of at least three rigid particles in point contact" that can support loads along its axis, with only small amounts of rotation allowed [19,20]. This so-called fixed principal axis model assumes that the directions of force chains coincide with the principal stress directions of the applied load. A similar observation has been made in biaxial compression tests in both two-dimensional (2D) discrete element simulations and experiments on photoelastic disk assemblies: in particular, columnlike structures form parallel to the major principal stress direction of the applied load [21–23].

Despite the plethora of investigations on force chains, however, there is still no generally agreed quantitative definition of what constitutes a force chain. Hence, for a given granular assembly under load, there is no quantitative method by which to determine and characterize all the force

*Email address: John.F.Peters@erdc.usace.army.mil
†Email address: mayadm@gmail.com
‡Author to whom correspondence should be addressed. Email address: atordesi@ms.unimelb.edu.au

chains in the assembly. To illustrate, examples of definitions of force chains found in the literature are: a linear string of at least three rigid particles in point contact [19,20]; linear clusters of contacting grains at which compressive stress is concentrated [24], any set of nearly collinear disks carrying stress larger than the mean [25,26]; chainlike regions of large forces [16]; quasilinear particle assemblies where stress is concentrated [27].

The aim of this study is to establish a method by which force chains could be characterized quantitatively, using the discrete element method (DEM) [28]. Toward this end, key questions that need to be answered are the following. What is the best way of identifying force chains? The contact force vector fields are usually dense which makes their visualization restrictive and cumbersome. Therefore, is there a particle property that could be used to correctly identify the magnitude and direction of force chains? Moreover, what criteria should be used to quantitatively distinguish between a particle that is part of a force chain and one that is not?

In the past, the most common method used to examine force propagation and its key characteristics (e.g., force chains) is to visualize individual contact forces by lines, the thickness (or color) of which represents the magnitude of the contact force [5,13]. Moreover, in work involving 3D simulations of particle packing, force chains were classified by simply following the path of maximum contact force at each particle [29,30]. However, this could result in highly nonlinear chains. More recently, an alternative method using correlation functions has been developed [2]. This method, however, is based on probabilities obtained from statistical averages of a measure of particle stress, and does not provide a characterization of each force chain in a given state of the system.

In other simulations, a particle property was used. Examples include the particle's potential energy density [6], and also the difference in the principal stresses which was used to enable a direct comparison of force propagation between photoelastic disk experiments (e.g., [1,2,25,26]) and material point method simulations [31]. Luding [6] and Mattutis [32], in their studies of static piles using DEM simulations, noted that the orientation of the major principal stress axis is correlated with the structure of the contact network. However, they did not use this particle property to identify the magnitude and direction of force chains.

In terms of identifying which particles form part of a force chain, a variety of methods have been employed but these tend to be qualitative [13,25]. A quantitative method would require precise definitions of two key aspects of force chains. The first concerns the magnitude of the contact force, while the second pertains to the linearity (or quasilinearity) of the whole force chain. The magnitudes of contact forces within force chains, described as "large," are generally considered to be above the average magnitude for the whole assembly. This is so because a number of studies have shown that the "strong network," comprising those forces having above average magnitudes, has significantly different behavior from the "weak network," which is made up of those forces having average or below average magnitudes. While the strong network, typically consisting of less than 40% of contacts, is more anisotropic and carries the majority of the load, the weak network acts more like an interstitial liquid and provides support [13]. An attempt to include the concept of quasilinearity in the analysis of the force chain morphology has been somewhat *ad hoc*: the particle property used was a scalar quantity, therefore providing no information on the direction of force chains [25]. In other cases, the visualization of force chains is simply done by filtering out the average and below average forces and then leaving the viewer to interpret or find the force chains in the resulting network [13].

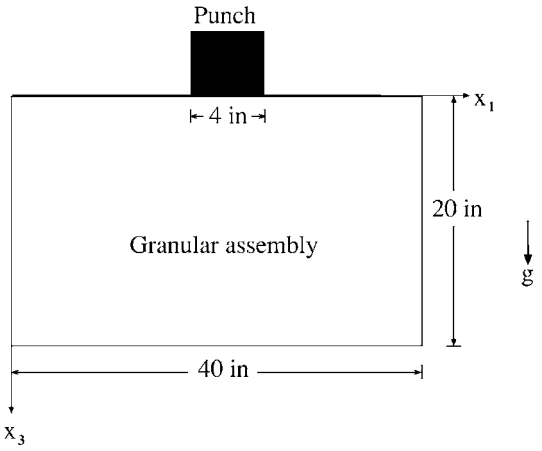

FIG. 1. The initial setup and dimensions of the flat punch system.

In this paper, a method is developed for the quantitative characterization of force chains. The numerical experiment used for the analysis is described in Sec. II. Next, a particle property that can be used to identify both the direction and magnitude of force chains is established in Sec. III. Criteria for the identification of force chains are presented in Sec. IV, with the corresponding algorithm in Sec. V. Results are presented in Sec. VI, followed by conclusions in Sec. VII.

II. THE NUMERICAL EXPERIMENT

The set of data on which this analysis was based has been generated from a discrete element simulation of a 2D granular assembly of polydisperse particles subject to indentation by a rigid flat punch [34]. The DEM code used is derived from earlier work by Horner *et al.* [33]. The initial packing distribution was created by randomly generating particles on a grid (with no contacts), then allowing them to fall into the box under gravity. Once the particles had settled, the top surface of the filled box was leveled off to create a flat surface on which to move the punch. The system, once again, was allowed to settle, until the average kinetic energy of the system was negligible (below 10^{-9} *J*). Figure 1 shows a schematic diagram of the initial setup, while Table I contains the parameters and material properties used. Simple contact laws based on Hooke's law in conjunction with Coulomb's law are used. After the system had settled, the punch was moved down until the final stage of indentation, i.e., 10% of the total height of the box.

III. MINOR PRINCIPAL STRESS FOR A PARTICLE

Using a recently developed particle visualization software [35], all contact forces between particles were visualized to

TABLE I. DEM parameters and material properties used.

Parameter	Value
Total indentation time	2 s
Time-step increment	1.843×10^{-5} s
Punch velocity	0.5 in./s(0.0127 m/s)
Box size	40×20 in.^{2}
	(1.016×0.508 m^2)
Punch width	4 in. (0.1016 m)
Number of particles	38 849
Particle density	0.2476 lb/in.^{3}
	(6854 kg/m^3)
Smallest radius	5.0×10^{-2} in.
	(1.27×10^{-3} m)
Largest radius	1.0×10^{-1} in.
	(2.54×10^{-3} m)
Average radius	7.5×10^{-2} in.
	(1.91×10^{-3} m)
Inter particle friction coefficient	0.1
Particle-wall friction coefficient	0.1
Rolling friction coefficient	0.1
Gravity value (in positive x_3 direction)	386.4 in./s^2
	(9.81 m/s^2)
Ratio of loading to unloading modulus	0.1
Normal spring stiffness constant	3000 lb/in.
	(5.25×10^5 N/m)
Tangential spring stiffness constant	3000 lb/in.
	(5.25×10^5 N/m)
Rotational spring stiffness constant	50 lb.in/rad
	(222 N.m/rad)

establish the network of force chains. Figure 2 shows all the contact forces between particles, for a small region of the particle assembly, at 10% indentation. Each contact force is drawn as a line, with the color of the line representing the magnitude of the force. The heterogeneity of the force network is clear, as are the quasilinear pathways of force transmission.

Our analysis shows that the particle property found to identify both the direction and magnitude of force chains is the most compressive principal stress. This quantity is derived from the particle stress tensor, which is defined in the usual way (e.g., [6,21,36]):

$$\sigma_{ij} = \frac{1}{V}\sum_{c=1}^{N^c} f_i^c r_j^c \tag{1}$$

where the summation runs over all contacts of the particle (that is, all external forces acting on the particle), V is the volume of the particle, N^c is the number of contacts of the particle, f_i^c the ith component of the force acting at the contact, and r_j^c the jth component of the radius vector from the center of the particle to the point of contact. The principal stresses are thus given by

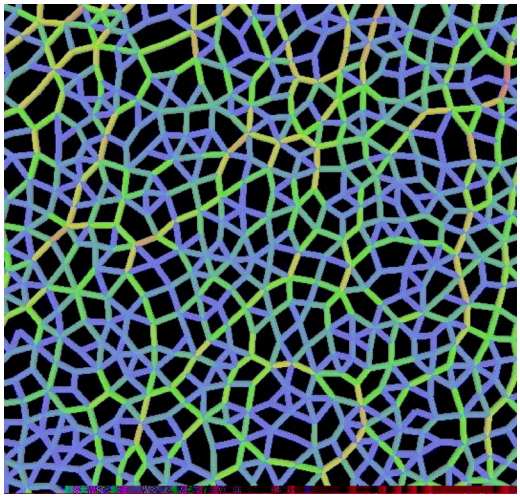

FIG. 2. (Color online) Contact forces between particles for a section of the particle assembly. The color of the force represents the magnitude, with light (red online) corresponding to large forces down to dark (blue online) representing small forces.

$$\sigma_1 = \frac{\sigma_{11}+\sigma_{33}}{2} + \sqrt{\left(\frac{\sigma_{11}-\sigma_{33}}{2}\right)^2 + (\sigma_{13})^2}, \tag{2}$$

$$\sigma_3 = \frac{\sigma_{11}+\sigma_{33}}{2} - \sqrt{\left(\frac{\sigma_{11}-\sigma_{33}}{2}\right)^2 + (\sigma_{13})^2}, \tag{3}$$

where the σ_{ij} are the components of the symmetric part of the particle stress, σ_1 is the major principal stress, and σ_3 is the minor principal stress. It should be noted that since the DEM code adopts a tension-positive convention, the minor principal stress is hence the most compressive principal stress. The direction of the major principal stress from the positive x_1 axis, θ, is given by

$$\tan(2\theta) = \frac{2\sigma_{13}}{\sigma_{11}-\sigma_{33}} \tag{4}$$

As illustrated in Fig. 3, the direction of the most compressive principal stress of the central particle points in the direction of the most compressive force, i.e., the direction of the force chain. Figure 4 shows the same region of particles as in Fig. 2, except that each particle is now represented by its minor principal stress σ_3. In Fig. 4, all particles are shown. However, in Fig. 5, only those particles with $|\sigma_3|$ greater than the average are shown: here, particles are represented as arrows, where the direction of the arrow is the direction of σ_3, and the color of the arrow represents the magnitude of σ_3. A direct comparison of Figs. 2 and 5 clearly shows that the particle property of minor principal stress captures both the magnitude and direction of force chains.

IV. CHARACTERIZING A FORCE CHAIN

Using the particle property of minor principal stress, an algorithm was developed to find all the force chains of a given system. This algorithm takes as input the contact information, as well as the particle principal stress information,

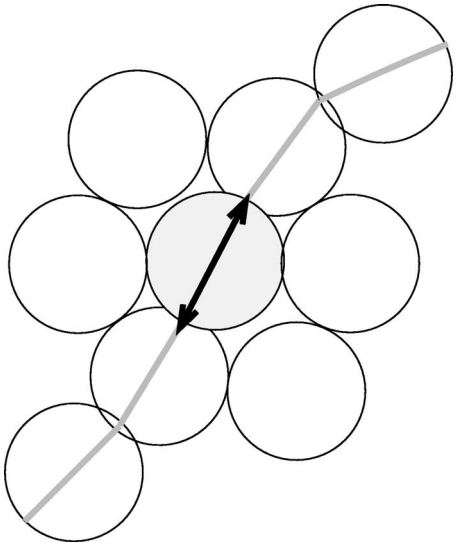

FIG. 3. Particles in an idealized portion of a force chain. The pathway of force transmission (force chain) is indicated by a gray line. The double-sided arrow through the particle center represents the direction of most compressive principal stress.

and produces various statistics (including whether or not particles are in force chains, the number of force chains, their lengths, etc.).

A definition of a force chain as a "quasilinear particle assembly where stress is concentrated" [27] was taken as a starting point for the algorithm, and was quantified in the following way.

Particle assembly. This refers to the fact that a group of particles is needed in order to form a chain. A single particle is clearly not a force chain, nor is a group of two particles. The proposed minimum number of particles required for an "assembly" is three. This value was also used in the fixed principal axis model [19,20].

Stress is concentrated. For particles to be in a force chain, they clearly must be experiencing large stresses compared to those particles not in chains. It is generally accepted [13] that only those contact forces with magnitudes greater than the

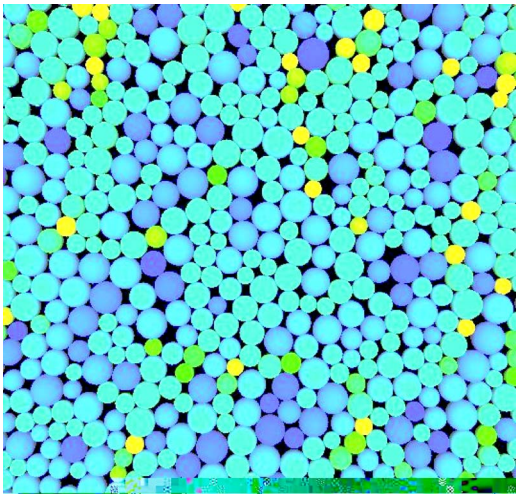

FIG. 4. (Color online) Particles colored by $|\sigma_3|$.

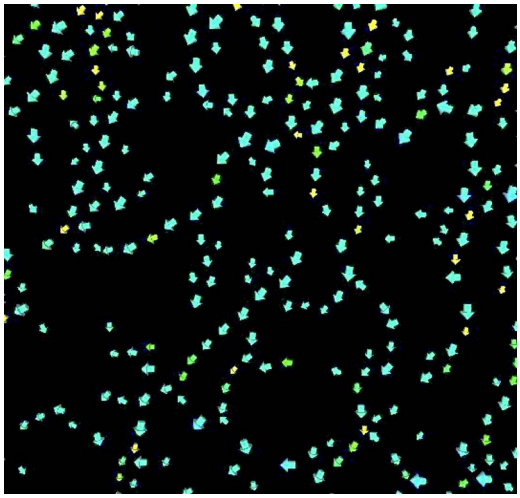

FIG. 5. (Color online) Particles represented by arrows, where the direction of the arrow is the direction of σ_3, and the color of the arrow is the magnitude of σ_3. Note that only those particles with $|\sigma_3|$ greater than the average are shown.

average (or equivalently, only those particles with stresses greater than the average) can be part of force chains. Therefore, we propose that particle j can only be part of a force chain if the magnitude of its minor principal stress, $|\sigma_3^j|$ is greater than the average:

$$|\sigma_3^j| > \frac{1}{N}\sum_{i=1}^{N} |\sigma_3^i| \tag{5}$$

where N denotes the number of particles, and $|\sigma_3^j|$ is the magnitude of the minor principal stress of particle i.

Quasilinear. We propose that the trajectories of the minor principal stresses of any candidate "assembly" must "line up." That is, although the assembly in Fig. 6(a) may be highly stressed, it would not be a force chain, since the directions of the minor principal stresses do not form a line. On the other hand, in Fig. 6(b), the highly stressed particle assembly would be a force chain.

V. THE ALGORITHM

Using the above quantifiable definition of a force chain, an algorithm was developed to find force chains in a system (see also the flowchart in Fig. 7).

(1) Read in contact information (to record each particle's neighbors) and principal stress information for all particles.

(2) Filter out all those particles with $|\sigma_3|$ less than or equal to the average.

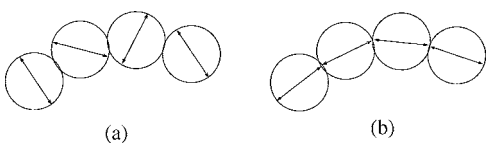

FIG. 6. Two assemblies of highly stressed particles that (a) do not and (b) do form a force chain.

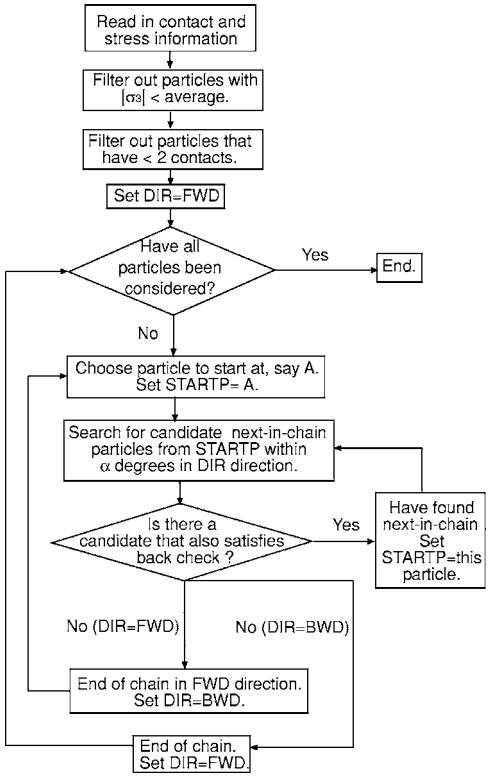

FIG. 7. A simplified flowchart of the algorithm (see Sec. V for more details).

(3) From these remaining highly stressed (where "highly stressed" refers to a particle having $|\sigma_3|$ greater than the average) particles, filter out all particles that are not in contact with any other highly stressed particles, and all particles that are only in contact with one other highly stressed particle.

(4) At this stage, only groups of three or more highly stressed particles remain. (a) Choose a particle, say, particle A in Fig. 8(a), and then find the next particle in the chain, if any. (b) Look in the forward direction of particle A's minor principal stress, σ_3^A, for candidate particles. Here, a parameter needs to be introduced that defines the angle used to search for contacts—α. An α value of 0 implies perfectly linear force chains, which is unrealistic in real systems. The α value used here was 45°, which allows force chains a reasonable degree of "curvature". Hence, it is first required that

$$\cos(\alpha) < \frac{|l\sigma_3^A|}{|l||\sigma_3^A|} \leqslant 1 \tag{6}$$

where $l=X_B-X_A$ is the branch vector from the center of particle A to the center of B. This means that any candidate particle must lie within $\alpha°$ to the left or right of the direction of σ_3^A. A graphical representation of this is in Fig. 8(b), where two candidates for the next particle (B and C) are found. (c) A situation might arise as in Fig. 8(c), where although particle B lies within particle A's allowed region, particle B's minor principal stress, σ_3^B, might not point back to particle A. To ensure this does not occur, a "back check" is performed, where the same constraint as explained above is used, except

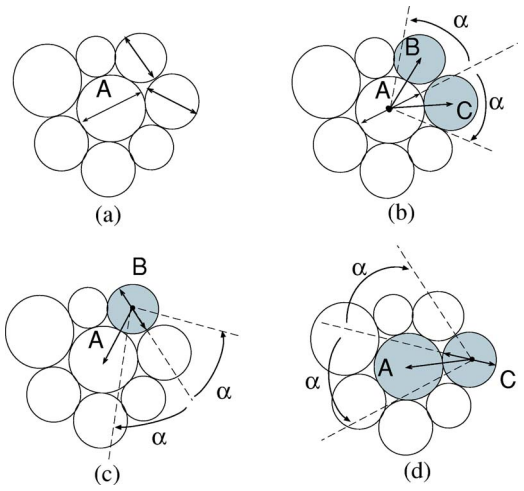

FIG. 8. (Color online) The algorithm used to find force chains. Double-sided arrows through particle centers indicate the direction of the minor principal stress. Single-sided arrows joining particle centers indicate branch vectors. (a) Start by choosing a particle to start at, particle A. (b) Look in the forward direction of particle A's minor principal stress, σ_3^A. Here two possibilities for the next particle in the chain are found (B and C). The angle α defines how far either side of σ_3^A to look. (c) Next, perform a back check: ensure that particle A lies within α deg of particle B's minor principal stress. In this case, it does not, so B is rejected as the next particle. (d) Performing a back checkfrom particle C is successful, so particle C is the next particle in the chain.

particles A and B are switched, that is, we require

$$\cos(\alpha) < \frac{|l'\sigma_3^B|}{|l'||\sigma_3^B|} \leqslant 1 \tag{7}$$

where $l'=X_A-X_B$ is now the branch vector from the center of particle B to the center of A. A graphical representation of this is in Figs. 8(c) and 8(d). (d) If both checks are satisfied, the next particle in the chain has been found (in Fig. 8, this is particle C). This loop is repeated, now starting at particle C. (e) Once all possible particles have been found in the forward direction of σ_3^A, this loop is repeated, except looking backward from particle A, to obtain all particles in the force chain containing particle A.

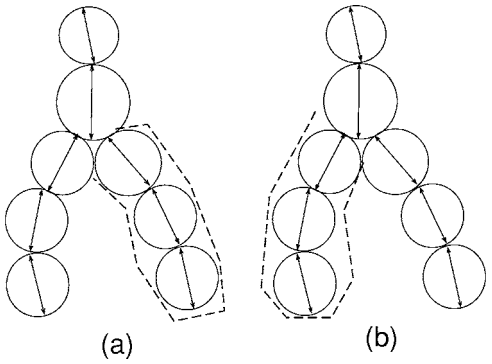

FIG. 9. A case where there exists two possibilities for force chains found by the algorithm.

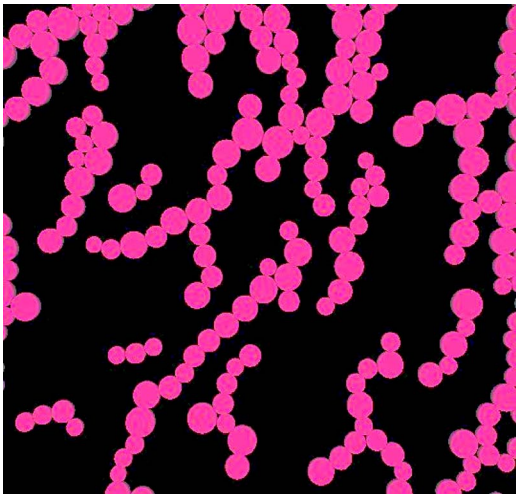

FIG. 10. (Color online) Force chains found by the algorithm—particles shown are part of a force chain.

This algorithm presents a first step toward identifying all force chains in a system. Notably, it does not incorporate force chain branching–if the algorithm comes to a branch point (that is, it has a choice between two possible next-in-chain particles), it will simply choose one branch to traverse, and the other branch will be traversed as part of a different force chain (see Fig. 9). A more detailed analysis of the force chain branch morphology and its evolution are currently being investigated.

VI. RESULTS

Figure 10 shows all the particles that are in force chains, for the same region of the system as in Figs. 2, 4, and 5. A comparison with actual contact forces between particles (Fig. 2) shows good agreement.

Figure 11 shows all particles for part of the assembly underneath the flat punch, at 10% indentation. Those particles colored red are part of a force chain, while those colored blue are not. Directly under the punch, the concentration of force chains is much greater, as more force chains have formed to counteract the load applied by the punch. These force chains tend to be aligned in the direction of applied stress [21].

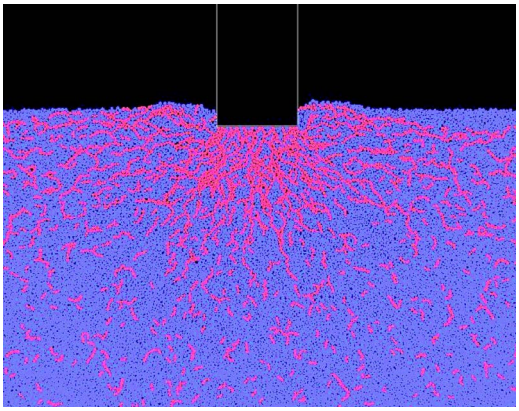

FIG. 11. (Color online) Force chains found underneath the flat punch—particles colored light (red online) are part of a force chain, while dark (blue online) particles are not.

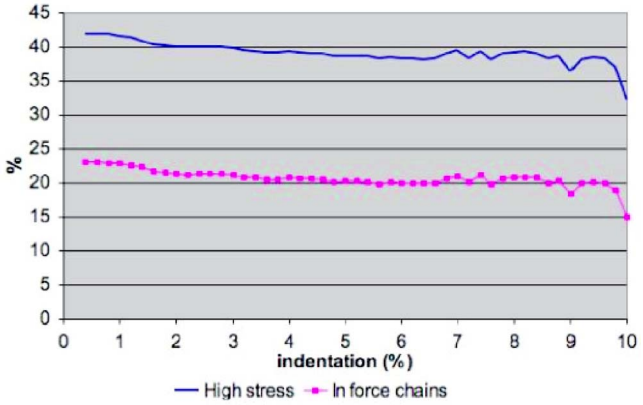

FIG. 12. (Color online) Evolution of the percentage of particles with $|\sigma_3|$ greater than the average ("high stress"), as well as the percentage of particles actually part of force chains.

Figure 12 shows the percentage of particles that have $|\sigma_3|$ greater than the average, as well as the percentage of particles that are actually part of force chains, as the punch indents. Interestingly, only approximately half of the particles in the strong network [13] are actually part of force chains. Note that the incorporation of branching into the present analysis may increase the percentage of particles that are part of force chains. However, this increase would be small as most of these highly stressed particles which are currently not part of any force chain exist either as a single particle in isolation or as isolated pairs (see, for example, Fig. 5).

Figures 13 and 14 show the number of force chains, and the average length of force chains, as the punch indents. A decrease in the total number of force chains is observed, which could be due to existing chains breaking down as the punch compresses. Also, note that the average length of force chains varies only slightly (between 4.55 and 4.75 particles in length) throughout deformation, and with no discernible pattern.

Figure 15 shows the distribution of lengths of force chains, for five different stages of indentation. The inset of a

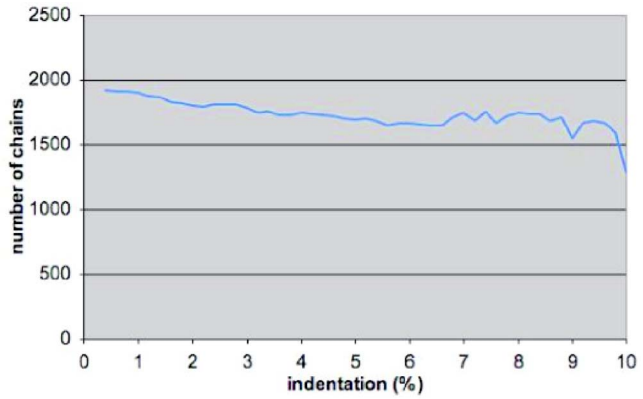

FIG. 13. (Color online) Evolution of the number of force chains found.

FIG. 14. (Color online) Evolution of the average length of force chains.

log plot of the length distribution shows that the distribution is exponential, for lengths up to approximately 11 particles.

VII. CONCLUSIONS

The main conclusions and findings of this research are the following.

(1) The particle property of most compressive principal stress (here the minor principal stress) was found to characterize both direction and magnitude of force chains.

(2) Using the vector property of minor principal stress, an algorithm was developed to find force chains in a given state of a system. This algorithm produces realistic force chains that correspond to actual strong contact force pathways.

(3) Initial results show that only approximately half of the particles in the strong network are actually part of force chains. Thus, assumptions that the strong network corresponds to, or is the same as, the force chain network cannot be made.

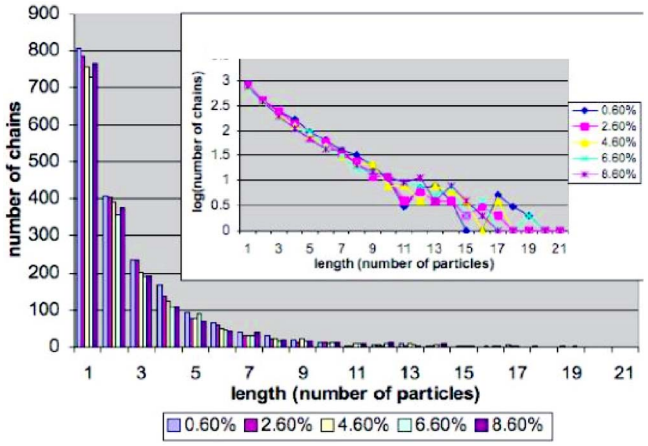

FIG. 15. (Color online) The distribution of lengths of force chains, for five different stages of indentation (%). Inset: Logarithmic plot demonstrating an exponential distribution.

(4) The average length of force chains was found to be approximately five particles. Clearly, this number depends on the searching angle α used in the force chain algorithm, and material properties (e.g., particle size and shape, packing distribution).

This investigation forms the basis for ongoing work aimed toward an understanding of the micromechanics of force chain evolution in deforming granular assemblies.

ACKNOWLEDGMENTS

The support of the U.S. Army Research Office through a grant to A.T. (Grant No. DAAD19-02-1-0216) is gratefully acknowledged, as is the University of Melbourne Advanced Research Computing section through a grant of computer time. This paper also reports on research conducted under the AT22 Research Project Stress Transfer in Granular Media conducted at the U.S. Army Engineer Research and Development Center.

[1] R. P. Behringer, D. Howell, L. Kondic, S. Tennakoon, and C. Veje, Physica D **133**, 1 (1999).
[2] J. Geng, G. Reydellet, E. Clement, and R. P. Behringer, Physica D **182**, 274 (2003).
[3] P. Dantu, Geotechnique **18**, 50 , (1968)(1968).
[4] F. Radjai, M. Jean, J. J. Moreau, and S. Roux, Phys. Rev. Lett. **77**, 274 (1996).
[5] F. Radjai, S. Roux, and J. J. Moreau, Chaos **9**, 544 (1999).
[6] S. Luding, Phys. Rev. E **55**, 4720 (1997).
[7] C.-H. Liu, S. R. Nagel, D. A. Schecter, S. N. Coppersmith, S. Majumdar, O. Narayan, and T. A. Witten, Science **269**, 513 (1995).
[8] S. N. Coppersmith, C. H. Liu, S. Majumdar, O. Narayan, and T. A. Witten, Phys. Rev. E **53**, 4673 (1996).
[9] C. Eloy and E. Clement, J. Phys. I **7**, 1541 (1997).
[10] J. E. S. Socolar, Phys. Rev. E **57**, 3204 (1998).
[11] J.-P. Bouchaud, M. Cates, and P. Claudin, J. Phys. I **5**, 639 (1995).
[12] S. Edwards and D. Grinev, Granular Matter **4**, 147 (2003).
[13] F. Radjai, D. E. Wolf, M. Jean, and J. J. Moreau, Phys. Rev. Lett. **80**, 61 (1998).
[14] C. Thornton and S. J. Antony, Powder Technol. **109**, 179 (2000).
[15] C. S. Chang and L. Ma, Int. J. Solids Struct. **28**, 67 (1991).
[16] R. Blumenfeld, Phys. Rev. Lett. **93**, 108301 (2004).
[17] J.-P. Bouchaud, P. Claudin, D. Levine, and M. Otto, Eur. Phys. J. E **4**, 451 (2001).
[18] J. E. S. Socolar, Discrete Contin. Dyn. Syst., Ser. B **3**, 601 (2003).
[19] M. E. Cates, J. P. Wittmer, J.-P. Bouchaud, and P. Claudin, Physica A **263**, 354 (1999).
[20] M. E. Cates, J. P. Wittmer, J.-P. Bouchaud, and P. Claudin, Phys. Rev. Lett. **81**, 1841 (1998).
[21] M. Oda and K. Iwashita, Int. J. Eng. Sci. **38**, 1713 (2000).
[22] K. Iwashita and M. Oda, Powder Technol. **109** 192 (2000).
[23] M. Oda, J. Konishi, and S. Nemat-Nasser, Geotechnique **30**,

479 (1980).
[24] C. D. V. Siclen, Physica A **333**, 155 (2004).
[25] D. Howell, R. P. Behringer, and C. Veje, Phys. Rev. Lett. **82**, 5241 (1999).
[26] D. W. Howell and R. P. Behringer, Chaos **9**, 559 (1999).
[27] C. S. Campbell, Granular Matter **5**, 129 (2003).
[28] P. A. Cundall and O. D. L. Strack, Geotechnique **29**, 47 (1979).
[29] H. A. Makse, D. L. Johnson, and L. M. Schwartz, Phys. Rev. Lett. **84**, 4160 (2000).
[30] N. Lacevic and S. C. Glotzer, J. Phys. Chem. B **108**, 19623 (2004).
[31] S. G. Bardenhagen, J. U. Brackbill, and D. L. Sulsky, Phys. Rev. E **62**, 3882 (2000).
[32] H. G. Mattutis, S. Luding, and H. J. Herrmann, Powder Technol. **109**, 278 (2000).
[33] D. A. Horner, J. F. Peters, and A. Carrillo, J. Eng. Mech. **127**, 1027 (2001).
[34] A. Tordesillas, J. F. Peters, and M. Muthuswamy, ANZIAM J. **46**, 260 (2005).
[35] University of Melbourne Software Engineering Department, report, 2003 (unpublished).
[36] G. Oron and H. J. Herrmann, Phys. Rev. E **58**, 2079 (1998).